J. Nanoanalysis., 5(2): 115-120 Spring 2018

ORIGINAL RESEARCH PAPER

Facile synthesis of Ni/NiO nanocomposites *via* thermal decomposition

Aliakbar Dehno Khalaji [1,*], Gholamhossein Grivani [2], Shaghayegh Izadi [2], Mehdi Ebadi [3]

[1] Department of Chemistry, Faculty of Science, Golestan University, Gorgan, Iran
[2] School of Chemistry, Damghan University, Damghan, Iran
[3] Department of Chemistry, Islami Azad University, Gorgan Branch, Gorgan, Iran

Received: 2017-09-20 Accepted: 2018-05-15 Published: 2018-06-30

ABSTRACT

In this study, Ni/NiO nanocomposites were prepared using simple, environment-friendly and low-cost solid-state thermal decomposition method from nickel (II) Schiff base complex at 400 and 500°C for 3 hours. The Ni/NiO nanocomposites were characterized with Fourier transformed infrared spectroscopy (FT-IR), X-ray powder diffraction (XRD), transmission electron microscopy (TEM) and X-Ray fluorescence (XRF). Results of XRD and XRF confirmed that the nanocomposite products contain a mixture of nickel and nickel oxide. The Ni or NiO content varied with the temperature used for the synthesis. Upon increasing the temperature from 400 to 500°C, the amount of NiO was found to be increased due to a complete oxidation of Ni to NiO. The TEM images demonstrated that the composites were spherical with a distribution size of about 10-30 nm. In addition, the products displayed reasonable electrochemical performance.

Keywords: *Ni/NiO Nanocomposites, TEM, Thermal Decomposition, XRD*

© 2018 Published by Journal of Nanoanalysis.

How to cite this article
Dehno Khalaji AA, Grivani GH, Izadi S, Ebadi M. Facile synthesis of Ni/NiO nanocomposites via thermal decomposition. J. Nanoanalysis., 2018; 5(2): 115-120. DOI: 10.22034/jna.2018.541868

INTRODUCTION

Because of its unique properties, Ni/NiO nanocomposites exhibit interesting properties such as thermal stability [1], magnetic properties [2,3] and applications in lithium ion batteries [4-8], electrocatalysts for hydrogen evolution reaction [9] and electrochemical energy storage [10] as a robust catalyst for the hydrogenation of levulinic acid to γ-valerolactone [11]. These properties have a direct correlation with the grain size, morphology and crystalline phases of Ni/NiO nanocomposites [1-21]. It is essential to prepare Ni/NiO nanocomposites with various morphologies and sizes. To date, several methods [1-21], such as chemical dealloying method [12], thermal annealing of Ni nanowires [13], a combination of chemical and gaseous reduction [15], citric acid assisted pechini-type method [20], one step solution combustion method [18], hydrothermal assiste polyol process [16], simple sol-gel [17], electrostatic spray deposition (ESD) [7], physical deposition method [8] and calcination of various precursors [5,6,22] have been developed to synthesize nano-sized Ni/NiO nanocompoistes. Mahendraprabhu and Elumalai [17] synthesized Ni/NiO nanocomposites by simple sol-gel process and reported the effect of citric acid on the formation of Ni/NiO nanocomposites. The results show that in lower nanoparticles:citric acid molar ratio (1:1 and 2:1), a mixture of Ni and NiO and in higher molar ratio, single phase of NiO was obtained. Gokul *et al.* [17] prepared Ni/NiO nanocomposites by hydrothermal-assisted polyol process and reported annealing

* Corresponding Author Email: *alidkhalaji@yahoo.com*

This work is licensed under the Creative Commons Attribution 4.0 International License.
To view a copy of this license, visit http://creativecommons.org/licenses/by/4.0/.

temperature on the magnetic properties of Ni/NiO nanocomposites. The results indicate that with increase of annealing temperature, the structure of Ni/NiO nanocomposite changed to NiO due to the transformation of Ni to NiO. Farzeneh and Kashanie [19] prepared Ni/NiO nanocomposites from mixture of $Ni(CH_3COO)_2.4H_2O$, acetylacetone and water under reflux condition, followed by the calcination at 400 °C and studied the elimination of congo red from aqueous solution. Results show that 95% of Congo red was eliminated at 497 nm after 30 min. Prabhu *et al.* [18] synthesized Ni/NiO nanocomposites synthesized by one step solution combustion method. They reported that the Ni or NiO content in the products varies with the quantity of HNO_3 used for the synthesis.

Recently, we used various Ni(II) Schiff base complexes as new precursor for preparing NiO nanoparticles by solid state thermal decomposition as simple, low cost and environmentally friendly [23,24]. Here, we used nickel (II) Schiff base complex (Scheme 1) and reported the synthesis of Ni/NiO nanocomposites using thermal decomposition method at 400 and 500 °C. The product characterized with FT-IR, XRD, SEM, TEM and XRF. In addition, electrochemical properties of the prepared nanocomposites were investigated

MATERIALS AND METHODS

Materials and measurements

All materials were commercially available and used without further purifications. Fourier transform infrared (FT-IR) spectra were recorded as a KBr disk on a FT-IR Perkin–Elmer spectrophotometer. X-ray powder diffraction (XRD) pattern of the complex was recorded on a Bruker AXS diffractometer D8 ADVANCE with Cu-Kα radiation with nickel beta filter ranging between $2\theta = 10^{o}–80^{o}$. The transmission electron microscopy (TEM) images were obtained from a JEOL JEM 1400 transmission electron microscope with an accelerating voltage of 120 kV. The X-ray fluorescence (XRF) was performed using a Skyray Instrument EDX3600H. Electrical energy saving properties of the synthesized nickel (II) Schiff base complexes were characterized by cyclic voltammetry (CV) and Galvanostatic charge/discharge techniques. While three compartment electrodes were used, Pt sheet (1×1 cm^2) as a counter, the fixed synthesized nickel (II) Schiff base complexes (2 mg) on the copper plate (1×1 cm^2) as a working and Ag/AgCl as reference electrodes were used in the 0.5 M Na_2SO_4 medium. Cyclic voltammetry was done in the potential rang of 0.1- (-0.7) V vs. Ag/AgCl at the variety scan rates (10-100 mV s^{-1}), while the charge/ discharge were performed at -5 - +5 and -4 - +4 mV using potantiostat/galvanostat (Autolab 302N).

The nickel(II) Schiff base complex was synthesized in methanol described elsewhere [25]. With continuous stirring, a solution of 2-aminophenol (4 mmol) in the 15 mL of CH_3OH was added to a solution of 4-dimethylaminobenzaldehyde (4 mmol) in CH_3OH (10 mL). In order to give a clear orange solution, the mixture was stirred at room temperature for about 45 min. Then, a solution of nickel acetate tetrahydrate (2 mmol) in methanol (15 mL) was added to this solution. While stirring, the resulting mixture was heated to evaporate the solvents to get precipitate of dark red nickel(II) Schiff base complex. The precipitate was washed with cold ethanol and dried at room temperature for several days. Yield: 65%. *Anal.* Calcd. for $C_{30}H_{30}N_4O_2Ni$: C.; 67.07 (66.95), H.; 5.59 (5.64), N.; 10.43 (10.39). FT-IR (KBr, cm^{-1}): 2877-3031 (C-H aromatic and aliphatic), 1586 (-C=N-), 1451 – 1557 (-C=C- aromatic).

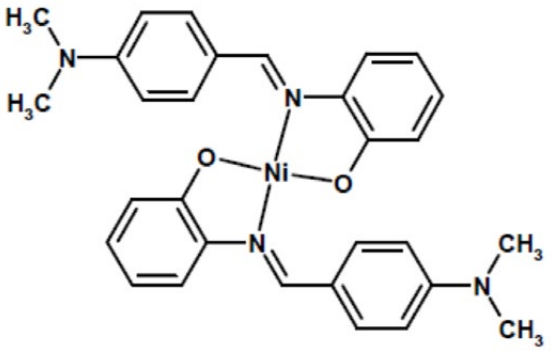

Scheme 1. Chemical structure of nickel(II) Schiff base complex

Preparation of Ni/NiO nanocomposites

For preparation of Ni/NiO nanocomposites, 0.5 gr of nickel(II) Schiff base complex is loaded into a crucible and then placed in the electrical furnace and heated at a rate of 10°C/min in air, follow by a calcination at 400 and 500°C for 3 h. Nanoparticles of Ni/NiO nanocomposites are produced, washed with ethanol and dried at room temperature. FT-IR (KBr, cm^{-1}): 458 (Ni-O) for Ni/NiO product at 400°C and 462 (Ni-O) for Ni/NiO product at 500°C.

Electrochemical study

Ni/NiO particles (S_{400} and S_{500}) were obtained by calcination of the synthesized nickel (II) Schiff base complexes at 400 and 500 °C, respectively. Electrical energy saving properties of S_{400} and S_{500} were characterized by cyclic voltammetry (CV) and Galvanostatic charge/discharge techniques. While three compartment electrodes were used, Pt sheet (1 × 1 cm2) as a counter, the fixed Ni/NiO particles (S_{400} and S_{500}) (2 mg) on the copper plate (1 × 1 cm2) as a working and Ag/AgCl as reference electrodes were used in the 0.5 M Na_2SO_4 medium. Cyclic voltammetry was done in the potential range of 0.1- (-0.7) V *vs*. Ag/AgCl at the variety scan rates (10-100 mV s^{-1}) whereas the charge/ discharge were performed at -5 - +5 and -4 - +4 mV using potentiostat/galvanostat (Autolab 302N). It should be mentioned that the Ni/NiO particles were fixed on the Copper plates using Silver conductive paste (Sigma-Aldrich)

RESULTS AND DISCUSSION

FT-IR spectra

Figs. 1 and 2 show FT-IR spectra of Ni(II) Schiff base complex and Ni/NiO nanocomposites, respectively. In the FT-IR spectra of complex, the peak at about 3000 cm^{-1} was assigned to C-H aliphatin and aromatic and the peaks at 1586 cm^{-1} was assigned to iminic group (C=N). The peak at about 458 cm^{-1} for Ni/NiO obtained from 400 °C and at about 461 cm^{-1} for Ni/NiO obtained from

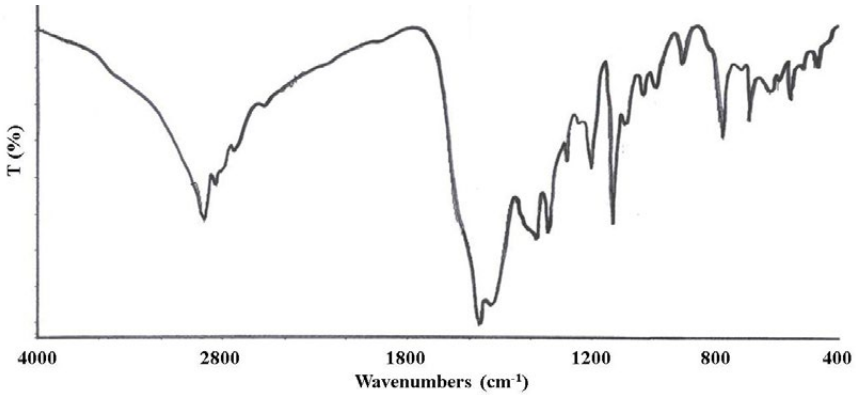

Fig. 1. FT-IR spectra of the Schiff base ligand and its Ni(II) complex.

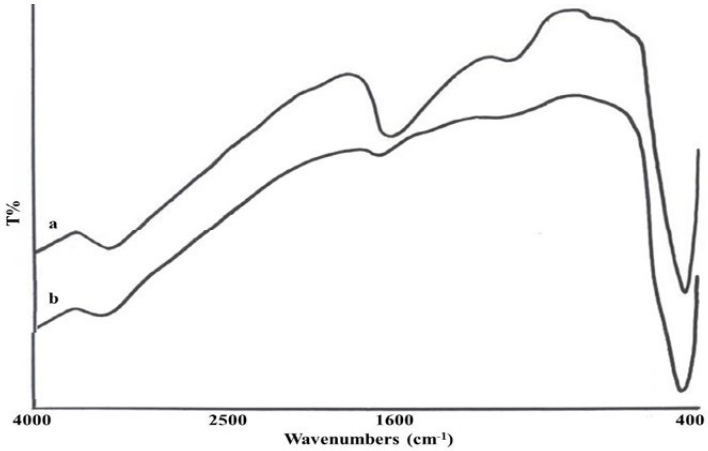

Fig. 2. FT-IR spectra of the prepared Ni/NiO nanocomposites at a) 400 °C and b) 500 °C.

500 °C that was assigned to the Ni-O stretching vibration mode [22,23], while the two peaks appeared 1610 and 3421 cm^{-1} for Ni/NiO obtained from 400 °C and 1637 and 3448 cm^{-1} for Ni/NiO obtained from 500 °C could be assigned to O-H stretching and binding vibration of H_2O molecules adsorbed on the surface of Ni/NiO, respectively [22, 23].

XRD patterns

XRD patterns of Ni/NiO nanocoposites (Fig. 3) show five obvious diffraction peaks located at about 37, 43, 63, 75 and 80° and agree with hexagonal structure of NiO [4-7] with lattice constant a = b = 2.955, c = 7.223 Å and space group R-3m. Furthermore, two diffraction peaks located at about 44 and 52° agree with cubic structure of Ni [4-7] with lattice constant a = b = c = 3.528 Å and space group Fm3m. The intensity of the characteristic peaks of the Ni phase decrease considerably as the temperature increases from 400 to 500°C, due to the oxidation of Ni to NiO [13,16]. The crystallite size was calculated using Debye-Scherrer formula and was found to be 24.6 and 24.1 nm, based on the NiO(012) plane and 24.5 nm, based on the Ni(111) plane, with an increase in decomposition temperature from 400 to 500 °C [13,16]. Results suggest that crystallinity of the Ni cubic structure was slightly greater than that of NiO hexagonal structure. The increasing of the decomposition temperature had no appreciable effect on the crystallite size of the prepared Ni/NiO nanocomposites.

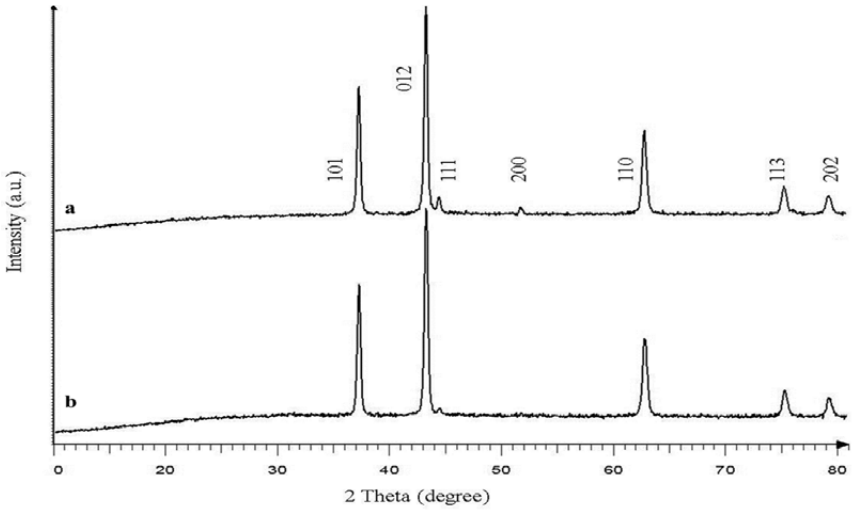

Fig. 3. XRD patterns of the prepared Ni/NiO nanocomposites at a) 400 °C and b) 500 °C.

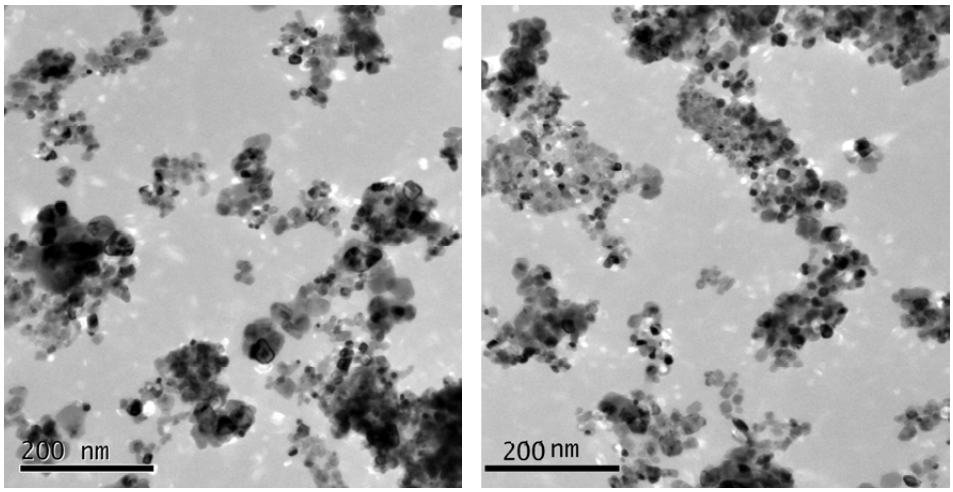

Fig. 4. TEM images of Ni/NiO nanocomposites prepared at 400 (left) an at 500 °C (right).

CC BY

TEM images

Fig. 4 depicts TEM images of Ni/NiO nanocomposites prepared at 400 and 500 °C. Comparison between TEM images confirmed that there is no difference between the morphology of the products. Relative fraction of metallic Ni was recorded by XRF and was found to be 19 and 7%, for Ni/NiO nanoparticles prepared at 400 and 500 °C, respectively. These results indicate that the products should be composite of metallic nickel and nickel oxide [13,16].

Electrochemical Studies

Electrochemical behavior of the Fixed Ni/NiO particles (S_{400} and S_{500}) on the copper plates were evaluated by Cyclic Voltammetry technique as shown in Figs. 5a and c, respectively. It was found that the curve areas increased due to the enhancement of scan rates. It means that linearly the curve area of voltammograms was a function of scan rate (v). Figs. 4b and d illustrate the linear relationship between curves area and scan rates (0.5 V). It was demonstrated that the electrochemical behavior of the fixed Ni/NiO particles on the copper plates for S_{400} and S_{500} were different.

The synthesized Ni/NiO particles at 500 °C (S_{500}) showed the linear behavior, while the synthesized Ni/NiO particles at 400 °C (S_{400}) was deviated from linear behavior by the increased scan rates. It is notable that potential position of peaks was the same (S_{500}), whereas the potential position of the peaks were shifted in the synthesized S_{400} with increasing scan rates as shown in Figs. 5a and c, respectively. According to these results (both linearity and potential shift), it can be concluded that the electrochemical behavior of S_{500} was diffusion-controlled while the above-mentioned behavior was partially diffusion-controlled for S_{400}.

Ebadi *et al.* explained the kinetic and diffusion–controlled of the electrochemical behavior of process [24]. The specific capacitance of activated materials depends on scan rate and anodic or cathodic currents. It can be calculated by equation (C= i/ v.w) where i is the average cathodic or anodic current (A), v is the scan rate (V s^{-1}) and w is the mass of activated material (g).

As shown in Figs. 5a and b, CV results were verified by galvanostat charge/discharge test. The prepared electrodes (S_{400} and S_{500}) represented reasonable load and unload charge behavior for

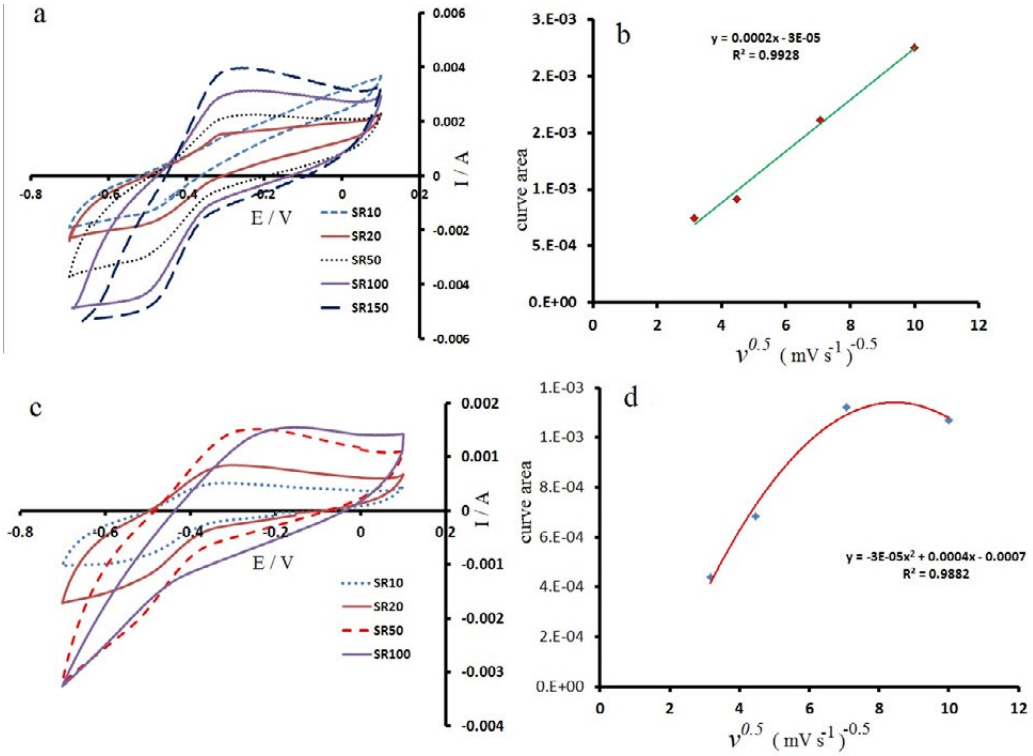

Fig. 5. a) Cyclic voltammograms of prepared electrodes as S_{500} at different scan rates (10–100 mV s^{-1}). b) Linear relationship between voltammogram areas vs scan rate for S_{500}. c) Cyclic voltammograms of prepared electrodes as S_{500} at different scan rates (10–100 mV s^{-1}). d) relationship between voltammogram areas vs scan rate for S_{400}.

CC BY

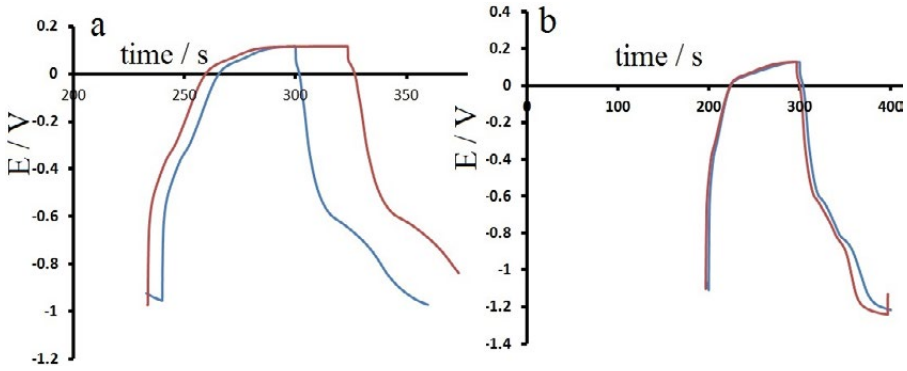

Fig. 6. a) Charge-discharge curves of (a) S_{500} (b) S_{400} at ±5 and ±4 mV current.

both applied currents (±5 and ±4 mV) in the 0.5 M Na_2SO_4. Both cases showed that the loading time were faster than unloading time for S_{500}, while it did not change for S_{400}

CONCLUSION

The Ni/NiO nanocomposites with various mass ratio between Ni and NiO were prepared and characterized. XRD and XRF results revealed that the amount of metallic Ni decreases due to oxidation to NiO upon increasing the temperature from 400 to 500 °C. In addition, SEM results showed that increasing the temperature increases the agglomeration of nanoparticles. The synthesized nanocomposites at different temperatures suggested different electrochemical behavior as S500 was diffusion-controlled and S400 was not entirely diffusion-controlled.

CONFLICT OF INTEREST

The authors declare that there is no conflict of interests regarding the publication of this manuscript.

REFERENCES

1. J. Kacher, P. Elizaga, S.D House, K. Hatter, M. Nowell, I.M. Robertson, Mater. Sci. Eng. A 568, 49-60 (2013).
2. S. Guo, W. Liu, H. Meng, X.H. Liu, W.J. Gong, Z. Han, Z.D. Zhang, J. All. Compd. 497, 10-13 (2010).
3. S. D'Addato, M.C. Spadaro, P. Luches, V. Grillo, S. Frabboni, S. Valeri, A.M. Ferretti, E. Capetti, A. Ponti, App. Surf. Sci. 306, 2-6 (2014).
4. Q. Xia, H. Zhao, Y. Teng, Z. Du, J. Wang, T. Zhang, Mater. Lett. 142, 67-70 (2015).
5. X.H. Huang, J.P. Tu, B. Zhang, C.Q. Zhang, Y. Li, Y.F. Yuan, H.M. Wu, J. Power Sources 161, 541-544 (2006).
6. P. Huang, X. Zhang, J. Wei, J. Pan, Y. Sheng, and B. Feng, Mater. Res. Bull. 63, 112-115 (2015).
7. X. Li, A. Dhanabalan, and C. Wang, J. Power Sources 196, 9625-9630 (2011).
8. X. Sun, W. Si, X. Liu, J. Deng, L. Xi, L. Liu, C. Yan, O.G. Schmidt, Nano Energy 9, 168-175 (2014).
9. X. Yan, L. Tian, and X. Chen, J. Power Sources 300, 336-343 (2015).
10. X. Yan, X. Tong, J. Wang, C. Gong, M. Zhang, and L. Liang, Mater. Lett. 106, 250-253 (2013).
11. S. Song, S. Yao, J. Cao, L. Di, G. Wu, N. Guan, L. Li, Appl. Catal. B. 217, 115-124 (2017).
12. T. Liu, Y. Pang, X. Xie, W. Qi, Y. Wu, S. Kobayashi, J. Zheng, X. Li, J. All. Compd. 667, 287-286 (2016).
13. W. Xiang, Y. Liu, J. Yao, R. Sun, Phys. E. 97, 363-367 (2018).
14. H.A. Chaghouri, F. Tuna, P.N. Santhosh, P. J. Thomas, Solid State Commun. 230, 11-15 (2016).
15. B.B. Nayak, S. Vitta, A.K. Nigam, D. Bahadur, Thin Sol. Films 505, 109-112 (2006).
16. B. Gokul, P. Saravanan, V.T.P. Vinod, and M. Cernik, Powder. Technol. 274, 98-104 (2015
17. K. Mahendraprabhu, and P. Elumalai, J. Sol-Gel. Sci. Technol. 73, 428-433 (2015).
18. V. Ganeshchandra Prabhu, P.S. Shajira, N. Lakshmi, and M. Junaid Bushiri, J. Phys. Chem. Solids. 87, 238-243 (2015).
19. F. Farzaneh, and S.H. Kashani, J. Cer. Process. Res. 14, 673-676 (2013).
20. L.A. Garcia-Cerda, K.M. Bernal-Ramos, S.M. Montemayor, M.A. Quevedo-Lopez, R. Betancourt-Galindo, D. Bueno-Baques, J. Nanomaterials 1-6 (2011).
21. J. Kim, B.-H. Choi, M. Kang, Powder Tech. 249, 419-423 (2013).
22. A.D. Khalaji, and D. Das, Int. J. Bio-inorg. Hybr. Nanomater. 4, 59-64 (2015).
23. A.D. Khalaji, J. Ultrafine Grained Nanostruct. Mater. 48, 1-4 (2015).
24. M. Ebadi, W.J. Basirun, Y.-L. Sim, and M.R. Mahmoudian, Metal. Mate. Trans. A. 44, 5096-5105 (2013).
25. R.L. Lal, M. Mandal, L. Roy, J. Mukherjee, R. Bhawal, and K. Maiti, Ind. J. Chem. A 47, 1480-1485 (2008).